Molecular and Electronic Structure of Nitridocyanometalates of Chromium(V) and Manganese(V): A Combined Experimental and DFT Study

Jesper Bendix,*,† Robert J. Deeth,‡ Thomas Weyhermüller,† Eckhard Bill,† and Karl Wieghardt*,†

Max-Planck-Institut für Strahlenchemie, Stiftstrasse 34-36, D-45470 Mülheim an der Ruhr, Germany, and Department of Chemistry, University of Warwick, Coventry CV4 7AL, W. Midlands, England

Received August 12, 1999

The six-coordinate complexes $[M(N)(CN)_5]^{3-}$ (M = Cr, Mn) have been isolated as salts of robust rhodium amine complexes. $[Rh(en)_3][Mn(N)(CN)_5]\cdot H_2O$ (**1**) and $[Rh(tn)_3]$ $[Cr(N)(CN)_5]\cdot 2H_2O$ (**2**) have been characterized by single-crystal X-ray crystallography: **1** crystallizes in the hexagonal space group $P6_3$ with $a = b = 15.810(2)$ Å, $c = 13.844(3)$ Å, $V = 2996.8(8)$ Å^3, and $Z = 6$; **2** crystallizes in the orthorhombic space group *Pbcn* with $a = 9.723(1)$ Å, $b = 14.564(2)$ Å, $c = 31.498(4)$ Å, $V = 4460.3(8)$ Å^3, and $Z = 8$. In **1**, all the anions are oriented with their Mn≡N directions almost coparallel to the crystallographic 3-fold axis. Polarized single-crystal UV−vis spectroscopy of **1** confirms the validity of the Jørgensen−Ballhausen−Gray d-orbital splitting scheme with the lowest energy transition being $d_{xy} \rightarrow \{d_{yz},d_{zx}\}$. Single-crystal EPR spectroscopy of $[Cr(N)(CN)_5]^{3-}$ diluted into **1** shows the hyperfine (^{53}Cr) and super-hyperfine (^{14}N) tensors to be quite anisotropic with different major axes. For the hyperfine interaction we observe $A_{||} > A_{\perp}$, whereas, for the super-hyperfine interaction to the terminal nitrido ligand, the reverse ordering is found: $A_{\perp} > A_{||}$. The complexes $[M(N)(CN)_5]^{3-}$, *trans*-$[M(N)(CN)_4(py)]^{2-}$, and $[M(N)(CN)_4]^{2-}$ (M = Cr, Mn) were investigated by DFT methods. Good reproduction of the molecular structures, vibrational, and UV−vis spectra was obtained. However, pronounced differences between local density and gradient corrected functionals were observed in the description of the weak bonding to the ligands trans to the nitrido ligand. For the five-coordinate $[M(N)(CN)_4]^{2-}$ complexes the LUMO is predicted to be a strongly admixed $d_{z^2}(M)-p_z(M)$ hybrid.

Introduction

The recent synthesis of nitrido complexes of the first-row transition metals with spectroscopically innocent ligands such as cyanide[1] and saturated amines[2] has allowed investigations of the electronic structure of these systems. In earlier studies on the strongly axially compressed nitrido−amine complexes *trans*-[(cyclam)M(N)(X)] (M = Cr, Mn; X = μ-N_3, CH_3CN) a "1 + 3 + 1 orbital splitting scheme" (Figure 1) with almost degenerate $d_{x^2-y^2}$, d_{yz}, and d_{zx} orbitals was deduced. This can be considered to be a limiting case of the Jørgensen−Ballhausen−Gray d-orbital splitting scheme (also Figure 1) which was originally developed to account for the optical spectrum of the vanadyl moiety.[3] In the nitridocyanometalates of Cr and Mn discussed in this paper the $d_{x^2-y^2}$ orbital is expected to be destabilized compared to the above-mentioned nitrido−amine complexes resulting in an orbital splitting scheme resembling the Jørgensen−Ballhausen−Gray scheme. The lowest energy d−d transition in these systems is thus anticipated to be $d_{xy} \rightarrow \{d_{zx},d_{yz}\}$. The previously reported UV−vis spectrum of $[Cr(N)(CN)_4]^{2-}$ is remarkable by exhibiting a long and distinct vibronic progression on the first absorption band even in solution at ambient temperature. An interpretation in terms of excited-state geometry and a possible explanation for the qualitative difference to the spectrum of the six-coordinate analogue $[Cr(N)(CN)_5]^{3-}$ is offered.

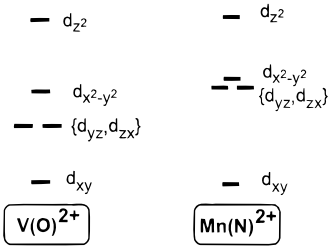

Figure 1. Orbital splitting diagrams for tetragonally compressed octahedral complexes with one (or two) axial strong σ- and π-donor ligands. Left-hand side: Traditional Jørgensen−Ballhausen−Gray scheme developed for the vanadyl moiety. The π-anisotropy raises the energy of the $\{d_{yz}, d_{zx}\}$ pair of orbitals compared to an octahedral system, and the σ-anisotropy lifts the degeneracy of the e_g set of orbitals by raising the energy of the d_{z^2} orbital. Right-hand side: near-degenerate situation previously deduced for *trans*-$[M(N)(cyclam)(X)]^{n+}$ systems.

The impressive success of density functional theory (DFT) in modeling the molecular and electronic structures of transition metal complexes[4] has been shown to extend to systems with multiply bonded ligands. For instance, Deeth has shown DFT to yield an accurate description of $[Cr(O)Cl_4]^-$,[5] vanadyl,[6]

† Max-Planck-Institut
‡ University of Warwick.

(1) Bendix, J.; Meyer, K.; Weyhermüller, T.; Bill, E.; Metzler-Nolte, N.; Wieghardt, K. *Inorg. Chem.* **1998**, *37*, 1767.
(2) (a) Meyer, K.; Bendix, J.; Metzler-Nolte, N.; Weyhermüller, T.; Wieghardt, K. *J. Am. Chem. Soc.* **1998**, *120*, 7260. (b) Meyer, K.; Bendix, J.; Bill, E.; Weyhermüller, T.; Wieghardt, K. *Inorg. Chem.* **1998**, *37*, 5180.
(3) (a) Jørgensen, C. K. *Acta Chem. Scand.* **1957**, *11*, 73. (b) Ballhausen, C. J.; Gray, H. B. *Inorg. Chem.* **1962**, *1*, 111.
(4) (a) Ziegler, T. *Chem. Rev.* **1991**, *91*, 651. (b) Deeth, R. J. *Struct. Bonding* **1995**, *82*, 1. (c) Chermette, H. *Coord. Chem. Rev.* **1998**, *178*, 699.
(5) Deeth, R. J. *J. Chem. Soc., Dalton Trans.* **1990**, 365.

10.1021/ic990971j CCC: $19.00
Published on Web 02/17/2000

molybdenyl,[7] and tetraoxometalate[8] complexes. Recently, DFT studies of nitridomolybdenum, -tungsten, and -technetium complexes[9,10] have demonstrated that the method yields accurate geometries and reliable d−d and charge transfer (CT) transition energies. Additionally, an electron density study on $[Cr^V(N)(bpb)]$ has shown DFT and experiment to agree well.[11] The calculation of individual term energies in systems with more than one d electron (or hole) by use of DFT has been employed successfully by Daul.[12] DFT modeling of the nitridocyanometalates of Cr and Mn is of interest in order to obtain an independent assignment of the electronic absorption spectra. Furthermore, these systems, which encompass the shortest metal−ligand bonds known, concomitant with normal-length bonds to the *cis*-cyanide ligands and extremely long bonds to the trans ligands, should also prove a valuable "litmus test" on the performance of DFT with respect to coordination geometries.

One recurring puzzle in the EPR-spectroscopic characterization of nitridochromium(V) complexes has been the apparently universal equivalence of the nitrido nitrogen atom and the nitrogen ligators of auxiliary ligands such as salen (H_2salen = *N,N′*-bis(salicylidene)ethane-1,2-diamine),[13] bpb (H_2bpb = 1,2-bis(pyridine-2-carboxamido)benzene),[14] cyclam (1,4,8,11-tetraazacyclotetradecane),[2] or porphyrins.[15] In these systems, the isotropic hyperfine couplings to the axial nitrido ligand and to equatorial N-donors have been found to be practically identical in magnitude. However, to date no examples have been reported where the superhyperfine coupling tensor to a nitrido ligand could be measured independently of couplings to other nitrogen nuclei.

Here we augment the studies on nitrido complexes with spectroscopically innocent auxiliary ligands by the structural and spectroscopic characterization of the pentacyanonitridometalates(V) of Cr and Mn. Additionally, DFT is applied to the known nitridocyano complexes of Cr^V, Mn^V, and Mn^{VI}.

Results and Discussion

The $[M(N)(CN)_5]^{3-}$ (M = Cr, Mn) complexes were previously shown to be accessible via ligand displacement on other nitrido complexes such as [M(N)(salen)] and isolated as the salts $Cs_2Na[M(N)(CN)_5]$ and $(NMe_4)_2Na[M(N)(CN)_5]\cdot H_2O$ (M = Cr, Mn).[1] However, neither of these types of salts yielded crystals suitable for X-ray structure analysis. Inspired by the classical use of robust am(m)ine complexes of tervalent cations as counterions for crystallization of trianions by Raymond and Basolo,[16] we have pursued the same strategy: Aqueous solutions of the rhodium ammine complexes $[Rh(NH_3)_6]^{3+}$, $[Rh(en)_3]^{3+}$, $[Rh(tn)_3]^{3+}$, and $[Rh(tacn)_2]^{3+}$ were allowed to slowly diffuse into solutions of $[M(N)(CN)_5]^{3-}$ containing excess cyanide ($[CN^-]$ = 0.5 M) whereupon crystalline precipitates were obtained in each case. Both $[Rh(en)_3][Mn(N)(CN)_5]\cdot H_2O$ (**1**) and $[Rh(tn)_3][Cr(N)(CN)_5]\cdot 2H_2O$ (**2**) gave X-ray-quality crystals the size of which were up to several millimeters in diameter.

Table 1. Selected Bond Distances (Å) and Angles (deg) for the $[M(N)(CN)_5]^{3-}$ (M = Cr, Mn) Complexes

	1	**2**		**1**	**2**
M−N(1)	1.499(8)	1.594(9)	M−C^{trans}(6)	2.243(7)	2.299(12)
M−C^{cis}(2)	1.988(7)	2.039(7)	C−N(av)	1.146(9)	1.109(13)
M−C^{cis}(3)	1.987(5)	2.08(2)	N−M-C^{cis}(av)	95.2(3)	97.1(3)
M−C^{cis}(4)	2.001(7)		N−M−C^{trans}	177.1(3)	180.0
M−C^{cis}(5)	1.985(6)				

Table 2. Metrical Data (Å) for Pairs of Analogous Cr^V and Mn^V Nitrido Complexes

complex	*d*(M≡N)	*d*(M−L^{trans})	*d*(out of plane)	ref
[Cr(N)(salen)]	1.544(3)		0.499	47
[Mn(N)(salen)]	1.512(3)		0.492	48
[Cr(N)(ttp)]	1.565(6)		0.42	49
[Mn(N)(oep)]	1.512(2)		0.430	50
trans-$[Cr(N)(cyclam)(NCCH_3)]^{2+}$	1.561(3)	2.432(3)	0.265	2b
trans-$[Mn(N)(cyclam)(NCCH_3)]^{2+}$	1.518(5)	2.409(5)	0.253	2a
trans-$[Cr(N)(CN)_4(py)]^{2-}$	1.570(3)	2.542(4)	0.264	1
trans-$[Mn(N)(CN)_4(py)]^{2-}$	1.525(4)	2.472(4)	0.246	1

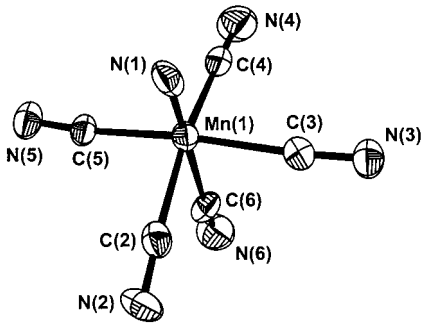

Figure 2. Structure of the $[Mn(N)(CN)_5]^{3-}$ anion in **1**. (Cf. Table 1 for metrical data.)

Crystal Structures. Compounds **1** and **2** were characterized by single-crystal X-ray crystallography. The resulting structural parameters are summarized in Table 1, and comparison with the metrical data for related systems is provided in Table 2. The structure of $[Mn(N)(CN)_5]^{3-}$ in **1** is shown in Figure 2. In crystals of **2** there are two different anion sites. One site holds an ordered anion the structure of which is qualitatively similar to that of the manganese analogue shown in Figure 2. The other site contains a statically disordered $[Cr(N)(CN)_5]^{3-}$ anion which is located close to a crystallographic inversion center. This disorder has been successfully modeled by a split atom model. In the following all references to the metrical data for the $[Cr(N)(CN)_5]^{3-}$ ion refer to the ordered site only. In both **1** and **2** the metal center in the anion is six-coordinate with the metal displaced out of the plane defined by the equatorial cyanide ligands toward the nitrido ligand, the displacement being 0.222 and 0.255 Å in **1** and **2**, respectively. These displacements are similar to those found for other six-coordinate M≡N complexes and are approximately half the magnitude of those found in five-coordinate Cr^V and Mn^V nitrido complexes (Table 2). The metal−nitride bond lengths are 1.499(8) and 1.594(9) Å in **1** and **2**, respectively. The difference in M−N bond length between the chromium and manganese systems is larger than normally found due to the unusually short Mn−N bond length in **1**. Comparison with related structures (Table 2) shows this anomaly. It is noteworthy that in neither **1** nor **2** is the terminal

(6) Deeth, R. J. *J. Chem. Soc., Dalton Trans.* **1991**, 1467.
(7) Deeth, R. J. *J. Chem. Soc., Dalton Trans.* **1991**, 1895.
(8) Deeth, R. J. *J. Chem. Soc., Faraday Trans.* **1993,** *89*, 3745.
(9) Baldas, J.; Heath, G. A.; Macgregor, S. A.; Moock, K. H.; Nissen, S. C.; Raptis, R. G. *J. Chem. Soc., Dalton Trans.* **1998**, 2303.
(10) Moock, K. H.; Macgregor, S. A.; Heath, G. A.; Derrick, S.; Boeré, R. T. *J. Chem. Soc., Dalton Trans.* **1996**, 2067.
(11) Wang, C.-C.; Wang, Y.; Chou, L.-K.; Che, C.-M. *J. Chem. Phys.* **1995**, *99*, 13899.
(12) (a) Daul, C.; Baerends, C. J.; Vernooijs, P. *Inorg. Chem.* **1994**, *33*, 3, 3538. (b) Gilardoni, F.; Weber, J.; Bellafrouh, K.; Daul, C.; Güdel, H. U. *J. Chem. Phys.* **1996,** *104*, 7624. (c) Doclo, K.; Corte, D. D.; Daul, C.; Güdel H. U. *Inorg. Chem.* **1998**, *37*, 3842.
(13) Arshankow, S. I.; Poznjak, A. L. *Z. Anorg. Allg. Chem.* **1981**, *481*, 201.
(14) Azuma, N.; Ozawa, T.; Tsuboyama, S. *J. Chem. Soc., Dalton Trans.* **1994**, 2609.
(15) Buchler, J. W.; Dreher, C.; Lay, K.-L.; Raap, A.; Gersonde, K. *Inorg. Chem.* **1983**, *22*, 879.
(16) (a) Raymond, K. N.; Basolo, F. *Inorg. Chem.* **1966**, *5*, 949. (b) Terzis, A.; Raymond, K. N.; Spiro, T. G. *Inorg. Chem.* **1970**, *9*, 2415.

nitrido ligand involved in hydrogen bonding. In **2** the shortest contact between a hydrogen bond donor and the nitrido ligand is 3.69 Å. Conversely, all of the cyano ligands are involved in hydrogen bonding to water molecules (2.94, 2.97 Å) or to the counterions (2.88, 2.99 Å). The trans cyano ligand, expected to be the most basic site, makes the shortest contact. The absence of hydrogen bonding to the terminal nitrido ligand is similar to the situation previously observed in $(PPh_4)_2[Mn(N)(CN)_4]\cdot 2H_2O$ and *trans*-$(PPh_4)_2[M(N)(CN)_4(py)]\cdot H_2O$ (M = Cr, Mn) and demonstrates that the nitrido ligand has a low basicity.

The present complexes are the first examples of structurally characterized nitrido complexes of first-row transition metals with identical monodentate cis and trans ligands and are therefore useful reference systems for the trans-influence in these systems. Very long bonds to the trans-situated cyanide ligand are found in both **1** and **2**. The $Mn-CN^{trans}$ bond length in **1** even exceeds that found in $[Mn^{II}(CN)_4]^{2-}$ (2.16 Å)[17] by a large margin. On the other hand, the M−C bond lengths of the equatorial cyanides are similar to those (1.95−2.02 Å) found in other six-coordinate $Mn^{II}-Mn^{IV}$ cyano complexes.[18,19,20] Likewise, the mean $Cr-CN^{cis}$ bond length in **2** is identical to that found in $[Cr(CN)_6]^{3-}$.[21] The trans influence measured by the bond-length difference $M-CN^{trans} - M-CN^{cis}$ is 0.25 Å in **1** and 0.24 Å in **2**. These values are much larger than those found for other axial pentacyano complexes of the metals in question: cf. 0.08 Å in $[(CN)_5Mn(\mu\text{-}O)Mn(CN)_5]^{6-}$ and 0.04 Å in $[Cr(NO)(CN)_5]^{3-}$.[22,23] However, in the rhenium analogue $[Re(N)(CN)_5]^{3-}$ the trans influence is larger, with $Re-CN^{trans} = 2.386$ Å and average $Re-CN^{cis} = 2.10$ Å.[24] This is opposite to the trend observed for the tetracyano complexes *trans*-$[Re(N)(CN)_4(H_2O)]^{2-}$ ($d_{Re-O} = 2.496(7)$ Å), *trans*-$[Tc(N)(CN)_4(H_2O)]^{2-}$ ($d_{Tc-O} = 2.559(9)$ Å), and $[Mn(N)(CN)_4]^{2-}$ (5-coordinate from H_2O solution).

In the hexagonal crystals of **1**, the Mn−N vectors of the anions are symmetry related through a crystallographic 3-fold axis and a parallel 2-fold screw axis. As a result, the Mn−N vectors make a small common angle of 9.4° with the crystallographic *c*-axis. The packing of the anions is depicted in Figure 3.

Polarized UV−Vis Spectroscopy. The crystals of **1** develop mostly in the shape of small single- or double-ended pencils, with an easily discernible 6-fold axis. This axis was found to coincide with the crystallographic *c*-axis. When viewed under a polarizing microscope, the crystals display pronounced dichroism: with the 6-fold axis of the crystals parallel to the electric field vector of the light, the crystals appear light-pink whereas they are deep red-purple in the perpendicular polarization. Polarized single-crystal spectra of **1** are shown in Figure 4. In the local C_{4v} symmetry of the $[Mn(N)(CN)_5]^{3-}$ anions transitions of symmetry A_1 and E will be electric dipole allowed in parallel and perpendicular polarization, respectively. The ground state of the $[Mn(N)(CN)_5]^{3-}$ complex, and of all other nitrido-

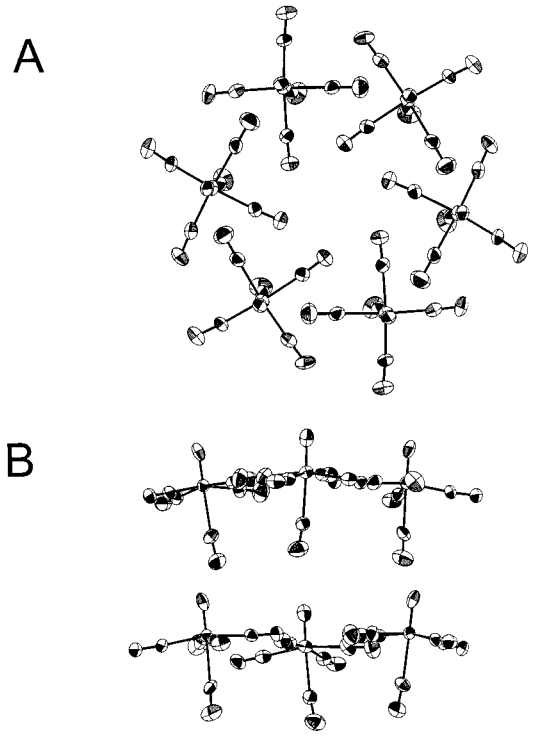

Figure 3. Anion packing in **1** seen along the 3-fold axis (top) and in the perpendicular direction (bottom).

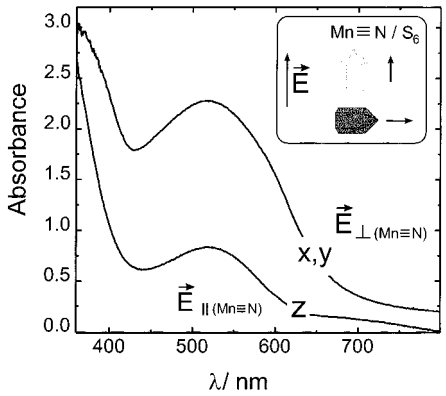

Figure 4. Polarized single-crystal spectra of **1**. The insert shows the morphology and the appearance of the crystals under a polarizing microscope.

manganese(V) complexes, is the spin-paired configuration $(d_{xy})^2$, which becomes a $^1A_1(C_{4v})$ state. It follows that the symmetries of the excited states to which transitions are electric dipole allowed are likewise A_1 and E. Because of the perpendicular polarization of the absorption band at 516 nm this band is proven to arise from a transition to an ^1E (C_{4v}) state. The lowest energy ^1E state corresponds to the strong-field configuration $(d_{xy})^1(d_{yz},d_{zx})^1$, which is the lowest state expected from the orbital splitting schemes of Figure 1. The observed polarization ratio of ~3 is much smaller than the value of $\cos(9.4°)^2/\cos(80.6°)^2 \approx 36$ expected on the basis of the structural data.

The higher energy transition (351 nm) observed as a shoulder in the solution spectrum of $[Mn(N)(CN)_5]^{3-}$ could not be observed in the crystal spectra due to the optical density of the handable crystals. On the basis of the insensitivity of that band toward the nature of the trans ligand, it was previously assigned as the $d_{xy} \rightarrow d_{x^2-y^2}$ transition, which fits well with the present confirmation that the first band is $d_{xy} \rightarrow \{d_{zx},d_{yz}\}$.

Single-Crystal EPR Spectroscopy. Although it was not possible to obtain pure crystals of the chromium analogue of **1**,

(17) Buschmann, W. E.; Arif, A. F.; Miller, J. S. *Angew. Chem., Int. Ed. Engl.* **1998**, *37*, 781−783.
(18) Tullberg, A.; Vannerberg, G. *Acta Chem. Scand.* **1974**, *A28*, 551.
(19) (a) Witzel, M.; Ziegler, B.; Babel, D. *Z. Naturforsch.* **1988**, *43B*, 1311. (b) Buschmann, W. E.; Liable-Sands, L.; Rheingold, A. L.; Miller, J. S. *Inorg. Chim. Acta* **1999**, *284*, 175.
(20) Buschmann, W. E.; Vazquez, C.; Ward, M. D.; Jones, N. C.; Miller, J. S. *Chem. Commun.* **1997**, 409.
(21) Güdel, H. U.; Stucki, H.; Ludi, A. *Inorg. Chim. Acta* **1973**, *7*, 121.
(22) Ziolo, R. F.; Stanford, R. H.; Rossman, G. R.; Gray, H. B. *J. Am. Chem. Soc.* **1974,** *96*, 7910.
(23) Enemark, J. H.; Quinby, M. S.; Reed, L. L.; Steuck, M. J.; Walthers, K. K. *Inorg. Chem.* **1970**, *9*, 2397.
(24) Purcell, W.; Potgeiter, I. Z.; Damoense, L. J.; Leipoldt, J. G. *Transition Met. Chem.* **1991**, *16*, 473.

Table 3. Summary of EPR Parameters of Nitridochromium(V) Complexes

parameter	$Cr(N)(CN)_5]^{3-}$	*trans*-[Cr(N)-(cyclam)$(NCCH_3)]^{2+}$ [a]	[Cr(N)(pbp)][b]	[Cr(N)salen)][b]	[Cr(N)(OEP)], [Cr(N)(TPP)][c]
g_{iso}	1.990	1.9856	1.983	1.978	1.9825
$A_{iso}(^{53}Cr)$, mT	2.49	2.80	2.84	2.83	2.827
$A_{iso}(^{14}N)$, mT	0.29	0.23	0.23	0.25	0.277
$g_{\|\|}$	1.9755	1.965	1.965	1.951	1.9583
$g_\perp$	1.9990	1.997	1.992	1.991	1.9945
$\langle g \rangle$	1.9912	1.986	1.980	1.978	1.9824
$A_{\|\|}(^{53}Cr)$, mT	3.89	4.20	4.41	4.81	4.01
$A_\perp(^{53}Cr)$, mT	1.50	1.60	2.21	1.98	2.24
$\langle A \rangle$ (^{53}Cr), mT	2.30	2.47	2.90	2.92	2.83
$A_{\|\|}(^{14}N)$, mT	0.09(6)				0.13 (ENDOR)
$A_\perp(^{14}N)$, mT	0.36				0.37 (ENDOR)
$\langle A \rangle(^{14}N)$, mT	0.27				0.29 (ENDOR)

[a] Reference 2b. [b] Reference 25. [c] Reference 15.

we found that doping of paramagnetic $[Cr(N)(CN)_5]^{3-}$ into diamagnetic crystals of **1** was possible. Crystalline samples of Cr-doped **1** were prepared from solutions containing 1−2% of Cr. The EPR spectrum of a microcrystalline sample of Cr-doped **1** at 300 K shows an axial signal (Figure 5A) with limited information content. The low-field absorption belongs to the $M_I = {}^3/_2$ component of the ^{53}Cr (9.5%) hyperfine quadruplet. Large single crystals of the doped material were grown by slow diffusion. Such a single crystal was mounted in an EPR tube with its *c*-axis perpendicular to the axis of rotation (tube). Spectra were recorded for orientations covering the full unique range of angles between the Cr−N direction and the B_0 field direction of the spectrometer. The results of these measurements are shown in Figure 5B. With the applied field parallel to the crystallographic 3-fold axis the spectrum consists of a single line originating from the Cr isotopes without nuclear spin surrounded by four lines originating from the coupling to ^{53}Cr. In the perpendicular direction only the outer lines of the ^{53}Cr quadruplet are discernible, but here an additional splitting into three of the central lines as well as of the $^{53}Cr(M_I = {}^3/_2)$ line occurs due to superhyperfine coupling to ^{14}N. All of the spectra originating from different orientations could be satisfactorily fitted with the single set of spin-Hamiltonian parameters given in Table 3. Spectral fits are shown for the extreme orientations and one intermediate orientation in Figure 6.

The $g_\perp$ value is close to the free electron *g*-value and close to the $g_\perp$ values determined for the other known Cr(V)−nitrido complexes. On the other hand, $g_{||}$ is significantly larger than $g_{||}$ values for other Cr(V)−nitrido complexes. With reference to the perturbation expression[3b]

$$g_{||} = g_e\left(1 - \frac{4\xi_{3d}}{E(d_{x^2-y^2}) - E(d_{xy})}\right)$$

this implies that the energy of the $d_{x^2-y^2}$ orbital is significantly higher in energy than in complexes with equatorial and O donors, a reasonable result given the position of cyanide in the spectrochemical series. Calculation of the spin−orbit coupling constant from the above expression and the energy of the second transition in the electronic spectrum yields a value of 93 cm^{-1} to be compared with 88 cm^{-1} previously determined for $[Cr(N)(cyclam)(NCCH_3)]^{3+}$.[2b] The hyperfine coupling tensor components, $A_{||}(^{53}Cr)$ and $A_\perp(^{53}Cr)$, are smaller than for the other known nitridochromium(V) complexes indicating the cyano complexes to be more covalent. The anisotropy of $A(^{53}Cr)$ in chromium(V) complexes has been discussed at length in the literature;[14,25] $[Cr(N)(CN)_5]^{3-}$ is unexceptional in this respect. The orientation averaged superhyperfine coupling is slightly larger than in similar systems but, importantly, of the same magnitude. This unequivocally establishes the EPR equivalence of the equatorial and apical nitrogen ligators in other $Cr{\equiv}N^{2+}$ complexes as accidental. The direct determination of the anisotropy of the superhyperfine coupling is only precedented by the ENDOR data of Buchler et al.[15] given in the last column of Table 3. Our data agree well with these. As previously noted,[25] all d orbitals except the d_{z^2} are mixed with the SOMO (d_{xy}) by spin−orbit coupling in tetragonal symmetry. The intuitively strongest interaction pathway between the electron spin and the nuclear spin of the nitrido ligand, the σ-bond, is thus ineffective, which justifies the small observed superhyperfine coupling. The absence of spin density in the d_{z^2} orbital and concomitantly in the $p_z(N)$ orbital is in perfect agreement with the observed strong anisotropy in the superhyperfine coupling

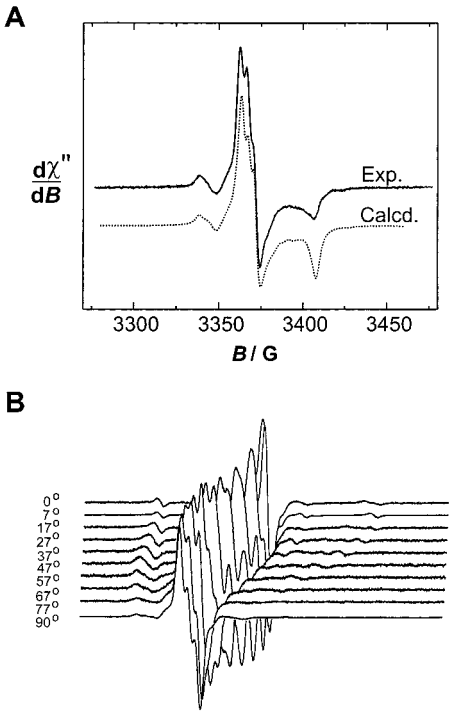

Figure 5. Powder (A) and single-crystal (B) EPR spectra of chromium-doped **1** containing ca. 1% Cr(V). Conditions: $T = 300$ K; $\nu = 9.4227$ GHz; microwave power = 2 mW. Note that the calculated powder spectrum is not a simulation of the experimental powder spectrum but obtained by simulation of a powder with the parameters extracted independently from the single-crystal spectra (cf. Figure 6 and Table 3).

(25) Azuma, N.; Imori, Y.; Yoshida, H.; Tajima, K.; Li, Y.; Yamauchi, J. *Inorg. Chim. Acta* **1997**, *266*, 29.

Table 4. Optimized and Experimental Geometries

		M−N (Å)	M−C (Å)	M−L^{trans} (Å)	C−N (Å)	N−M-C (deg)
$[Cr(N)(CN)_4]^{2-}$	LDA	1.530	2.010		1.169	103.9
	GC	1.545	2.065		1.176	103.6
$[Mn(N)(CN)_4]^{2-}$	expt	1.507(2)	1.974(20)		1.160(1)	105.1(6)
	LDA	1.502	1.934		1.170	104.5
	GC	1.517	1.980		1.177	103.5
$[Mn^{VI}(N)(CN)_4]^{-}$	LDA	1.500	1.920		1.165	104.3
	GC	1.516	1.965		1.172	103.7
$[Cr(N)(CN)_5]^{3-}$	expt	1.594(9)	2.06(1)	2.299(12)	1.109(13)	97.1(3)
	LDA	1.570	2.046	2.318	1.173	95.5
	GC	1.581	2.116	2.438	1.179	94.4
$[Mn(N)(CN)_5]^{3-}$	expt	1.499(8)	1.990(6)	2.243(7)	1.146(9)	95.2(3)
	LDA	1.543	1.961	2.204	1.174	96.1
	GC	1.549	2.020	2.348	1.180	95.3
tr-$[Cr(N)(CN)_4(py)]^{2-}$	expt	1.570(3)	2.077(3)	2.542(4)	1.162(7)	99.3(1)
	LDA	1.541	2.023	2.528	1.170	100.5
	GC	1.552	2.078	2.812	1.177	101.3
tr-$[Mn(N)(CN)_4(py)]^{2-}$	expt	1.525(4)	1.994(7)	2.472(4)	1.158(2)	98.8(2)
	LDA	1.515	1.941	2.467	1.171	99.7
	GC	1.523	1.991	2.817	1.178	101.7

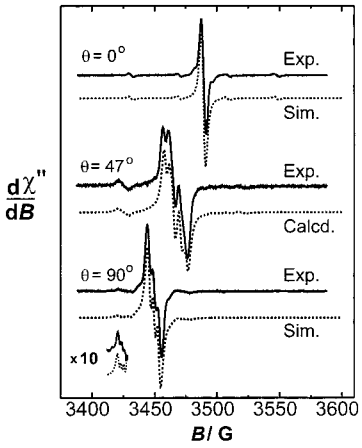

Figure 6. Simulated single-crystal EPR spectra. For parameters cf. Table 3. Note that the simulation of the middle spectrum is without any degrees of freedom employing the parameters extracted from the spectra corresponding to the extreme orientations.

and the following ordering: $A_{||}(^{14}N) < A_{\perp}(^{14}N)$. Since symmetry prevents a Fermi contact mechanism from being operative (no spin density in the a_1 valence orbitals on the metal) it can be concluded that the superhyperfine interaction to the terminal nitrido ligand occurs via a spin-polarization mechanism via the set of π-orbitals (d_{yz},d_{zx}) on the metal. The observed strong anisotropy of the superhyperfine coupling is a consequence of the asymmetric surroundings of the nitrido ligand and the covalency of the metal−ligand bond. In both respects the present systems are paralleled by the known terminal phosphido complexes of molybdenum and tungsten. For these systems Cummins et al. have shown the shielding of the phosphorus nuclei to be exceedingly anisotropic.[26]

DFT Calculations. We have computed the optimized geometries for all known nitrido cyano complexes of Mn and Cr using the local density approximation (LDA) and gradient-corrected (GC) density functional theory. Table 4 lists the calculated and experimental data. Both LDA and GC calculations reproduce the very short metal−nitrido distances well. The exception is the $[Mn(N)(CN)_5]^{3-}$ ion for which both methods calculate a M−N bond 0.05 Å longer than the experimentally found. However, the calculations are more in line with chemical intuition and the general trends observed for the complexes and the small discrepancy is most likely caused by an underestimated distance in the X-ray structure. The difference between LDA and GC calculated M−N bond lengths is significantly smaller than for normal metal−ligand bonds. This is also shown by the calculated bond lengths for the equatorial cyanide ligands. Here the difference between LDA and GC calculations amounts to 0.05−0.07 Å, which is in the range normally observed for Werner-type complexes.[27] An underestimation (overbinding) of the bond length by LDA and a good agreement with GC is found for the equatorial cyanide ligands which make these "organometallic" in their DFT behavior according to the classification in ref 27. For the very weakly bonded trans ligands the picture is drastically different: LDA performs surprisingly well for both pyridine and cyanide trans ligands with a maximal error of 0.04 Å. With the Becke−Perdew gradient-corrected functional, on the other hand, the M−CN^{trans} bond length in the $[Mn(N)(CN)_5]^{3-}$ ions is overestimated by 0.14 and 0.11 Å for Cr and Mn, respectively. The discrepancy is yet larger for the weakly bonded pyridine complexes, being 0.27 and 0.34 Å for the Cr and Mn complexes, respectively. To examine if this is a feature specific to the employed gradient corrections, we geometry-optimized the *trans*-$[Mn(N)(CN)_4(py)]^{2-}$ complex with all of the different gradient-corrected functionals implemented in the ADF program package. The result was that the B88+P86 gradient corrected functional actually was the best performing among these. Thus PW91 was 0.68 Å and B88-LYP was 0.44 Å off. This finding parallels that of Delley et al.,[28] who found the B88-P86 functional among several gradient-corrected functionals to give the best agreement with experimental geometries for selected carbonyl complexes. The trans ligands in question are very weakly bonded, and therefore, packing forces are most likely capable of modulating the experimentally determined bond lengths to some extent. However, the consistent performance of LDA and increasing discrepancy in the GC results with increasing bond lengths signals a warning concerning the use of the standard GC functionals for weak bonds in coordination complexes. The optimized geometries are practically independent of the oxidation state of the metal in the $[Mn(N)(CN)_4]^{2-/-}$ pair.

As pointed out in the discussion of the hydrogen-bonding patterns in the hydrated nitridocyanometalate salts, there is

(26) Wu, G.; Rovnyak, D.; Johnson, M. J. A.; Zanetti, N. C.; Musaev, D. G.; Morokuma, K.; Schrock, R. R.; Griffin, R. G.; Cummins, C. C. *J. Am. Chem. Soc.* **1996**, *118*, 10654.

(27) Bray, M. R.; Deeth, R. J.; Paget, V. J.; Sheen, P. D. *Int. J. Quantum Chem.* **1996**, *61*, 85.

(28) Delley, B.; Wrinn, M.; Lüthi, H. P. *J. Chem. Phys.* **1994**, *100*, 5785.

Table 5. Calculated Charge and Spin Densities (LDA)[a]

	metal	(N)	C^{cis}	N^{cis}	L^{trans}
$[Cr(N)(CN)_4]^{2-}$	+0.01	−0.37	−0.03	−0.38	
	(1.10)	(−0.18)	(−0.04)	(0.06)	
$[Mn(N)(CN)_4]^{2-}$	−0.12	−0.33	+0.01	−0.40	
$[Mn^{VI}(N)(CN)_4]^{-}$	−0.03	−0.16	+0.07	−0.28	
	(1.00)	(−0.18)	(−0.04)	(0.08)	
$[Cr(N)(CN)_5]^{3-}$	−0.22	−0.45	+0.01	−0.46	-0.53
	(1.16)	(−0.21)	(−0.04)	(0.06)	(−0.01)
$[Mn(N)(CN)_5]^{3-}$	−0.39	−0.41	+0.05	−0.48	-0.48
tr-$[Cr(N)(CN)_4(py)]^{2-}$	−0.04	−0.39	0.00	−0.40	+0.03
	(1.11)	(−0.19)	(−0.04)	(0.06)	(−0.004)
tr-$[Mn(N)(CN)_4(py)]^{2-}$	−0.16	−0.34	+0.04	−0.43	+0.06

[a] Spin densities are in parentheses.

Table 6. Calculated and Experimental Vibrational Frequencies (cm^{-1})[a]

		ν(M−N)	ν(C−N)	ν(M−C)
$[Cr(N)(CN)_4]^{2-}$	expt	1054	2130	(484)
	LDA	1182	2144/2148	494
	GC	1138	2103/2105	459
$[Mn(N)(CN)_4]^{2-}$	expt	1094	2115/2126	(425)
	LDA	1220	2130/2150	439
	GC	1173	2087/2102	416

[a] The experimental data are from ref 1. The values in parantheses are for the corresponding $[M(N)(CN)_5]^{3-}$ ions.

experimental evidence for the fact that the nitrido ligand possesses very little basicity. This finding is nicely paralleled by the calculated charge distribution in these complexes. Table 5 lists the calculated atomic charges and shows that the nitrogen atoms of the cyanide ligands are calculated to have approximately the same negative charge as the nitrido ligand. In all cases the central metal is found to be nearly uncharged. This reinforces the conclusion previously reached for the nitrido ammine complexes of the same metals, which are not protonated in concentrated $HClO_4$, namely that the M≡N moiety is a unit and that charges derived by formal oxidation states are very formal.[2]

Also listed in Table 5 are the calculated spin densities for the d^1 systems. The spin distributions parallel those previously found for $[V^{IV}(O)(CN)_5]^{3-}$.[6] The difference in spin density on the nitrido ligand and on the cis ligators is larger than expected from the experimentally found EPR equivalence in systems with equatorial N-donors.[2b,14,25] However, the calculated spin density on the nitrido ligand is to an extent of 98% located in p orbitals, in excellent agreement with the ligand-field-based symmetry argument (vide supra) and the observed anisotropy ($A_\perp(^{14}N) > A_\parallel(^{14}N)$). The spin density on the equatorial ligators is more evenly distributed with ca. 42% in s orbitals.

The calculated and experimental IR frequencies are tabulated in Table 6. The metal−nitrido stretching frequency is calculated significantly too high with both LDA (ca. 130 cm^{-1}) and GC (ca. 80 cm^{-1}). However, the ordering of ν(M≡N) values for the Cr and Mn complexes as well as the absolute difference for the two metals is reproduced precisely. The calculated metal cyanide stretch and bend vibrations are in good agreement with the experiment with the LDA values being too high and the GC values too low.

In Table 7 the calculated transition energies and the experimental data are compiled. The calculations were all done using the optimized geometries. For the sake of consistency the electronic transition energies are reported for LDA calculations. In general, the d−d transitions are calculated too high in energy and the ct transitions too low. This is to some extent remedied by using gradient-corrected functionals (which invariably gave the same energetic orderings of the orbitals) where the longer optimized bond lengths result in lower d−d energies and higher ct energies. The effect is not very large (500−2000 cm^{-1}) on the ct energies but more important for the d−d transition energies (on average ca. 2500 cm^{-1} with the largest effect ca. 4900 cm^{-1} on the $2b_2 \rightarrow 5b_1$ transition, which is the one for which LDA is the most off). The discrepancies between calculated and observed $2b_2 \rightarrow 5b_1$ transition energies also diminish if the experimental geometries are employed and are thus mainly related to the underestimation of the equatorial cyanide bond lengths using LDA.

For all of the examined systems the correct number of observable d−d transitions is predicted even if the onset of ct transitions is generally predicted too early. Contrary to the situation for $[Cr(N)(CN)_4]^{2-}$, experimentally no d−d band is observed in the UV−vis spectrum of $[Mn^{VI}(N)(CN)_4]^{-}$. In the DFT description this difference is also reproduced. It is attributable to a larger stabilization (average 5.5 eV) of the metal d orbitals as compared to the filled ligand orbitals (ca. 4.2 eV) upon the increase in oxidation state. The closely spaced highest lying filled orbitals have both cyanide and nitride character (cf. Figure 7), and the observed LMCT transitions can thus not be ascribed to either type of ligand individually.

Different orbital splitting schemes and ordering of the electronic transitions were calculated for the five- and six-coordinate species. The orbital energy diagram for the $[Cr(N)(CN)_4]^{2-}/[Cr(N)(CN)_5]^{3-}$ pair is depicted in Figure 7. The results for the corresponding d^2 complexes are qualitatively similar. The $9a_1$ orbital in which the metal contribution has a large (60%) $Cr(3d_{z^2})$ character becomes the LUMO in the five-coordinate species. This comes about by mixing in metal-p_z orbitals (40% based on metal contributions; 17% overall), which directs the resulting hybrid toward the vacant coordination site and lowers the antibonding interaction with the filled s−p hybrid on the nitrido ligand. The $9a_1$ orbital of $[Cr(N)(CN)_4]^{2-}$ is shown in Figure 8. The large lobe is pointing away from the nitrido ligand, and complete annihilation of the constituent orbitals between the metal and the nitrido ligand is apparent.

The predicted different nature of the first excited state in the five- and six-coordinate complexes is interesting in conjunction with the qualitative difference in the electronic spectra of $[Cr(N)(CN)_4]^{2-}$ and the other known nitrido cyanometalates. Of these, only the former exhibits a very pronounced vibrational fine structure on the first d−d band. As discussed in ref 1 the spacing of the vibronic progression is in accordance with it being a relatively pure Cr−N stretch. We have made a standard Franck−Condon analysis[29] of the vibrational fine structure in the spectra of $[Cr(N)(CN)_4]^{2-}$, employing intensities from the absorption as well as from the MCD spectra of ref 1. From these data we deduce a Cr−N bond length elongation (assuming the progression to be in a pure Cr−N stretch, which is probably a rather crude assumption; vide infra) in the excited state of 0.05−0.07 Å. The range reflects different methods of estimation of the intensities of the individual vibronic components. To obtain model data suited for comparison, we have geometry-optimized the $[Cr(N)(CN)_4]^{2-}$ ion in the first and second excited states which correspond to the electronic transitions $2b_2 \rightarrow 9a_1$ and $2b_2 \rightarrow 8e$, respectively. These geometry optimizations (LDA) were carried out starting close to the C_{4v} optimized ground-state geometry but without any imposed symmetry restrictions to allow the Jahn−Teller instability of the 8e populated state to manifest itself. The optimized excited-state

(29) Ballhausen, C. J. *Theor. Chim. Acta* **1963**, *1*, 285.

Table 7. Calculated d−d and Charge Transfer Transition Energies (cm^{-1})[a]

	$[Cr^{V}(N)(CN)_4]^{2-}$	$[Mn^{VI}(N)(CN)_4]^{-}$		$[Mn^{V}(N)(CN)_4]^{2-}$
		d−d		
$2b_2 \rightarrow 9a_1$	25 050 (24 100)	28 590		19 560/17 460 (20 200)
$2b_2 \rightarrow 8e$	28 460	28 170		23 000/19 320 (28 500)
$2b_2 \rightarrow 5b_1$	33 750	38 980		36 510/30 330
		CT (LMCT)		
$7e \rightarrow 2b_2$	24 000 (>37 000)	13 650 (20 400)	$7e \rightarrow 9a_1$	35 660/34 520 (>37 000)
$6e \rightarrow 2b_2$	25 780	16 620 (22 600)	$6e \rightarrow 9a_1$	37 780/35 800
$1a_2 \rightarrow 2b_2$	28 420	15 020 (23 900)	$1a_2 \rightarrow 9a_1$	37 510/36 950
$8a_1 \rightarrow 2b_2$	27 450	20 180	$8a_1 \rightarrow 9a_1$	42 220/38 800
	$[Cr^{V}(N)(CN)_5]^{3-}$			$[Mn^{V}(N)(CN)_5]^{3-}$
		d−d		
$2b_2 \rightarrow 9e$	26 590 (23 300)			18 070/14 810 (19 400)
$2b_2 \rightarrow 5b_1$	31 790 (27 700)			34 190/26 990 (27 000)
$2b_2 \rightarrow 12a_1$	38 940			36 370/32 550
		CT (LMCT)		
$11a_1 \rightarrow 2b_2$	18 290 (35 800)		$11a_1 \rightarrow 9e$	30 520/26 820 (34 800)
$8e \rightarrow 2b_2$	21 200		$8e \rightarrow 9e$	34 840/28 440
$7e \rightarrow 2b_2$	26 230		$7e \rightarrow 9e$	37 420/36 900
$1a_2 \rightarrow 2b_2$	30 410		$1a_2 \rightarrow 9e$	41 100/41 160

[a] Experimental values are in parentheses.

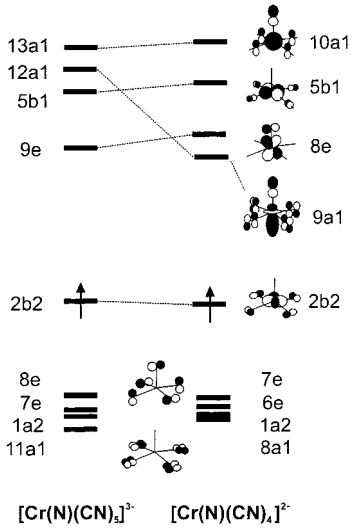

Figure 7. Orbital energy diagram the $[Cr(N)(CN)_5]^{3-}/[Cr(N)(CN)_4]^{2-}$ pair. The energies of the nonbonding $1a_2$ orbital have been chosen as the zero point of energy for both systems.

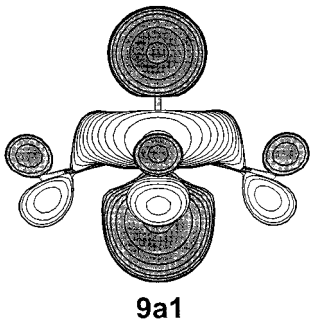

Figure 8. $9a_1$ orbital of $[Cr(N)(CN)_4]^{2-}$. (See text for discussion.)

geometries are shown in Figure 9. It is difficult to discriminate between the two possibilities on basis of the calculated elongation of the Cr−N bond (0.05 and 0.09 Å, respectively). These calculated distortions are somewhat counterintuitive inasmuch as the n → p* transition gives rise to a larger distortion than the transition which is *formally* n → s*. This clearly illustrates how admixing of p_z into d_{z^2} annihilates the σ-antibonding character with respect to the nitride ligand of the latter

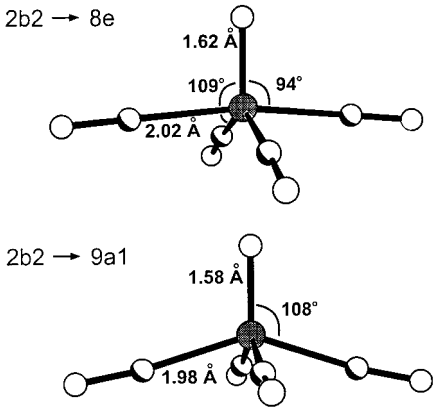

Figure 9. Optimized excited-state geometries for the two lowest excited states of $[Cr(N)(CN)_4]^{2-}$.

orbital (Figure 8). The relative magnitudes of the calculated distortions do not suggest that the $2b_2 \rightarrow 9a_1$ transition should be especially prone to exhibit vibrational fine structure. Favorable is, however, the excited-state geometry which corresponds predominantly to a Cr−N bond elongation with a modest admixture of Cr−CN bending. Attempts at geometry optimizing $[Cr(N)(CN)_5]^{3-}$ in the first excited state have all failed at the employed level of theory. The trans-situated cyanide ligand is dissociating in this state in good accordance with the photosensitivity of this complex.[1] This suggests that the absence of resolved vibrational fine structure for the pentacyano complexes is due to coupling to (dissociative) $M-CN^{trans}$ stretching. Noteworthy in the structure of the second ($2b_2 \rightarrow 8e$) excited state of $[Cr(N)(CN)_4]^{2-}$ is the pronounced Jahn−Teller distortion toward a (C_{2v}) trigonal bipyramid with the nitrido ligand in an equatorial position. Such a distortion was originally proposed by Gray and co-workers[30] for $[Os(N)(X)_4]^{-}$ (X = Cl, Br) on the basis of observation of a progression in the corresponding vibrational coordinate of b_1 symmetry. It remains to be understood why there is no resolved vibrational fine structure in the spectrum $[Mn(N)(CN)_4]^{2-}$, for which same ordering of the orbitals is calculated as for the Cr analogue.

(30) Hopkins, M. D.; Miskowski, V. M.; Gray, H. B. *J. Am. Chem. Soc.* **1986**, *108*, 6908.

The singlet−triplet splittings calculated for the manganese complexes are smaller than those experimentally observed for the nitrido(cyclam)manganese(V) complexes. For the latter complexes a Racah *B* value of 394 cm^{-1} was determined from a ligand field analysis. The values of *B* extracted[31] from the splittings in the DFT calculation on $[Mn(N)(CN)_5]^{3-}$ range from 150 to 420 cm^{-1} with an average of 311 cm^{-1}.

Conclusion

The crystal structures of **1** and **2** containing the $[M(N)(CN)_5]^{3-}$ (M = Cr, Mn) ions show that these have short terminal nitrido−metal bonds (1.5−1.6 Å). These M≡N groups display a large trans influence (ca. 0.25 Å) on the trans M···C bonds. Given the strength of cyanide as a ligand, this is probably a lower limit on the trans influence in these types of complexes. On the basis of the polarized single-crystal spectra, the first absorption band in $[Mn(N)(CN)_5]^{3-}$ can be unambiguously assigned as the $^1A_1((d_{xy})^2) \rightarrow {}^1E((d_{xy})^1(d_{zx},d_{yz})^1)$ transition. This assignment is in line with our previous suggestion based on the Jørgensen−Ballhausen−Gray splitting scheme and corroborates the orbital splitting scheme calculated by use of DFT for the six-coordinate nitridocyanometalates.

In $[Cr(N)(CN)_5]^{3-}$ the anisotropy of the superhyperfine coupling with $A_\perp(^{14}N)/A_\parallel(^{14}N) > 3$ makes the relatively weak coupling to the nitrido ligands in $Cr^V(N)$ complexes understandable. In agreement with symmetry considerations and DFT calculations, the experimentally determined anisotropy in the coupling indicates it to be mainly mediated by the π-bonding interaction. The molecular structure of the investigated complexes is reproduced well by DFT with the notable exception that common gradient corrected functionals seriously overestimate the trans influence of the nitrido ligand. The loosely bonded trans ligands in six-coordinate nitrido complexes of Cr and Mn can be envisaged as close to dissociating. Thus the failure of GC DFT for the bond lengths to these ligands may also be considered a warning concerning uncritical use of GC functionals in determining transition state geometries. The electronic structure of the nitridocyanometalates as described by DFT is in line with the understanding developed from ligand field considerations. However, DFT predicts extensive $d_{z^2}(Cr)-p_z(Cr)$ mixing in five-coordinate $[Cr(N)(CN)_4]^{2-}$, which provides a possible rationalization of the extensive vibrational fine structure of the first absorption band in the UV−vis spectrum and of the photosensitivity of this species. In a general treatment of transition metal pentacoordination[32] Hoffmann and Rossi pointed out the possibility of the d_{z^2} orbital becoming lower in energy than the degenerate set $\{d_{zx},d_{yz}\}$ in square pyramidal complexes but added a cautionary note in the introduction of their paper that it was legitimate to question some of the foundations of their model, such as the crucial role they assigned to hybridization with the $(n + 1)$p orbitals. We conclude by cautioning not to dismiss the possibility d−p mixing, which does indeed appear to be generally important in square pyramidal nitrido complexes.

Experimental Section

The starting materials $(NMe_4)_2Na[M(N)(CN)_5]\cdot H_2O$ (M = Cr, Mn) and $[Rh(tacn)_2]Br_3$ were prepared according to the published methods.[1,33] All of the salts described below were prepared analogously to **1** (the chromium complexes are photosensitive and were prepared in the dark). Details of the preparation are therefore only given once.

$[Rh(en)_3][Mn(N)(CN)_5]\cdot H_2O$ (1). Solutions of $[Rh(en)_3]Cl_3\cdot 3H_2O$ (120 mg, 0.27 mmol) in 3 mL of 0.5 M aqueous NaCN and $(NMe_4)_2Na[Mn(N)(CN)_5]\cdot H_2O$ (60 mg, 0.15 mmol) in 2 mL of 0.5 M aqueous NaCN were filtered through Millipore (HV; pore size 0.45 mm) filters and allowed to diffuse together through a glass frit. In 24 h red-violet pencil-shaped crystals of X-ray quality were collected and washed with a little ice-cold water and methanol. Yield: 45 mg (61%). IR (KBr disk), cm^{-1}: ν(CN), 2104, 2111 (vs), 2134 (m); ν(Mn−N), 1002 (s). Raman: ν(Mn−N), 1003 (s) cm^{-1}. Anal. Calcd for $C_{11}H_{26}MnN_{12}ORh$: C, 26.41; H, 5.24; N, 33.60; Mn, 10.98. Found: C, 26.52; H, 5.17; N, 33.84; Mn, 11.13.

$[Rh(tn)_3][Mn(N)(CN)_5]\cdot 2H_2O$. $[Rh(tn)_3]Cl_3$ (80 mg, 0.19 mmol) and $(NMe_4)_2Na[Mn(N)(CN)_5]\cdot H_2O$ (60 mg, 0.15 mmol) yielded 78 mg of product (94%). IR (KBr disk), cm^{-1}: ν(CN), 2108, 2121 (vs); ν(Mn−N), 1007, 989 (s). Raman: ν(Mn−N), 1007, 990 (m) cm^{-1}. Anal. Calcd for $C_{14}H_{34}MnN_{12}O_2Rh$: C, 30.01; H, 6.12; N, 30.00. Found: C, 29.65; H, 6.03; N, 29.84.

$[Rh(tacn)_2][Mn(N)(CN)_5]\cdot 4H_2O$. $[Rh(tacn)_2]Br_3\cdot 5H_2O$ (90 mg, 0.13 mmol) and $(NMe_4)_2Na[Mn(N)(CN)_5]\cdot H_2O$ (50 mg, 0.12 mmol) yielded 59 mg of product (76%). IR (KBr disk), cm^{-1}: ν(CN), 2107, 2117 (vs); ν(Mn−N), 1000 (vs). Raman: ν(Mn−N), 1001, 993 (m) cm^{-1}. Anal. Calcd for $C_{17}H_{38}MnN_{12}O_4Rh$: C, 32.29; H, 6.06; N, 26.58; Mn, 8.69. Found: C, 32.29; H, 5.89; N, 26.93; Mn, 8.82.

$[Rh(NH_3)_6][Mn(N)(CN)_5]\cdot 6H_2O$. $[Rh(NH_3)_6]Cl_3$ (75 mg, 0.24 mmol) and $(NMe_4)_2Na[Mn(N)(CN)_5]\cdot H_2O$ (50 mg, 0.12 mmol) yielded 38 mg of product (62%). IR (KBr disk), cm^{-1}: ν(CN), 2115 (vs), 2076 (m); ν(Mn−N), 989 (s). Raman: ν(Mn−N), 990 (s) cm^{-1}. Anal. Calcd for $C_5H_{30}MnN_{12}O_6Rh$: C, 11.72; H, 5.90; N, 32.81. Found: C, 11.77; H, 5.79; N, 33.14.

$[Rh(tn)_3][Cr(N)(CN)_5]\cdot 2H_2O$ (2). $[Rh(tn)_3]Cl_3$ (80 mg, 0.19 mmol) and $(NMe_4)_2Na[Cr(N)(CN)_5]\cdot H_2O$ (60 mg, 0.15 mmol) yielded 52 mg of product (63%). IR (KBr disk), cm^{-1}: ν(CN), 2093, 2121, 2134 (vs); ν(Cr−N), 968, 948 (s). Anal. Calcd for $C_{14}H_{34}CrN_{12}O_2Rh$: C, 30.17; H, 6.15; N, 30.15. Found: C, 29.98; H, 6.13; N, 30.21.

$[Rh(tacn)_2][Cr(N)(CN)_5]\cdot 4H_2O$. $[Rh(tacn)_2]Br_3\cdot 5H_2O$ (90 mg, 0.13 mmol) and $(NMe_4)_2Na[Cr(N)(CN)_5]\cdot H_2O$ (50 mg, 0.12 mmol) yielded 55 mg of product (70%). IR (KBr disk), cm^{-1}: ν(CN), 2103, 2121, 2127 (vs); ν(Cr−N), 961 (vs). Anal. Calcd for $C_{17}H_{38}CrN_{12}O_4Rh$: C, 32.44; H, 6.08; N, 26.70; Cr, 8.26. Found: C, 32.45; H, 6.03; N, 27.03; Cr, 8.34.

$[Rh(NH_3)_6][Cr(N)(CN)_5]\cdot 6H_2O$. $[Rh(NH_3)_6]Cl_3$ (75 mg, 0.24 mmol) and $(NMe_4)_2Na[Cr(N)(CN)_5]\cdot H_2O$ (50 mg, 0.12 mmol) yielded 51 mg of roduct (81%). IR (KBr disk), cm^{-1}: ν(CN), 2097, 2127 (vs); ν(Cr−N), 946 (m). Anal. Calcd for $C_5H_{30}CrN_{12}O_6Rh$: C, 11.79; H, 5.94; N, 33.00. Found: C, 11.88; H, 5.90; N, 33.27.

Calculations. DFT calculations were performed with the Amsterdam density functional (ADF) program suite version 2.3.0.[34,35,36] Slater-type orbital basis sets of triple-ζ quality for the valence orbitals were employed with polarization functions on the ligand atoms (2p for H and 3d for C and N) and additional valence p orbitals on the metal atoms (ADF basis set IV). Frozen core approximations were used up to 1s on C and N and up to 2p on the metals. The Vosko−Wilk−Nusair correlation functional was employed in the LDA calculations. In the GC calculations the exchange functional proposed by Becke (B88)[37] and the correlation functional due to Perdew (P86)[38] were used unless otherwise explicitly stated. To facilitate the calculations, the symmetries were restrained to C_{4v} for the $[M(N)(CN)_4]^{2-}$ and $[M(N)(CN)_5]^{3-}$ complexes and to C_{2v} for the *trans*-$[M(N)(CN)_4(py)]^{2-}$ complexes. All charge and spin densities were based on Mulliken

(31) The *B* values were calculated using the intermediate coupling scheme of $[Mn(N)(cyclam)(NCCH_3)]^{2+}$.[2a] In the intermediate scheme the following splittings apply (assuming $C = 4B$): $^1E-{}^3E = 14.4B$; $^1A_2-{}^3A_2 = 10.1B$; $^1B_2-{}^3B_2 = 14.6B$.

(32) Rossi, A. R.; Hoffmann, R. *Inorg. Chem.* **1975**, *14*, 365.

(33) Wieghardt, K.; Schmidth, W.; Nuber, B.; Prikner, B.; Weiss, J. *Chem. Ber.* **1980**, *113*, 36.

(34) ADF 2.3.0, Theoretical Chemistry, Vrije Universitet, Amsterdam.

(35) Baerends, E. J., et al. *Chem. Phys.* **1973**, *2*, 41.

(36) te Velde, G.; Baerends, E. J. *J. Comput. Phys.* **1992**, *99*, 84.

(37) Becke, A. D. *Phys. Rev.* **1988**, *A38*, 3098.

(38) Perdew, J. P. *Phys. Rev.* **1986**, *B33*, 8822; Perdew, J. P. *Phys. Rev.* **1987**, *B34*, 7406 (erratum).

Table 8. Crystallographic Data for the Complexes

	1	**2**
formula	$C_{11}H_{26}MnN_{12}ORh$	$C_{14}H_{34}CrN_{12}O_2Rh$
fw	500.29	557.44
space group	$P6_3$	Pbcn
a, Å	15.810(2)	9.723(1)
b, Å	15.810(2)	14.564(2)
c, Å	13.844(3)	31.498(4)
α, deg	90	90
β, deg	90	90
γ, deg	120	90
V, Å^3	2966.8(8)	4460(1)
Z	6	8
T, K	293(2)	100(2)
ρ_{calcd}, g cm^{-3}	1.663	1.660
no. of data	14159	34977
no. of unique data	4371	4350
no. of params	244	279
μ(Mo Kα), mm^{-1}	1.486	1.265
R1[a]	0.0590	0.0641
wR2[b]	0.1521	0.1366

[a] Observation criterion: $I > 2\sigma(I)$. $R1 = \sum||F_o| - |F_c||/\sum|F_o|$. [b] $wR2 = [\sum[w(F_o^2 - F_c^2)^2]/\sum[w(F_o^2)^2]]^{1/2}$, where $w = 1/\sigma^2(F_o^2) + (aP)^2 + bP$ and $P = (F_o^2 + 2F_c^2)/3$.

analyses.[39] Transition energies were calculated using both the ΔSCF and Slater's transition state method.[40] These invariably agreed to within 2000 cm^{-1}, and only those calculated by the latter method are quoted. For the d^2 systems, singlet and triplet energies were calculated by the method originally devised by Ziegler *et al.*[41] and further developed by Daul.[42]

EPR, Vibrational, and Electronic Spectra. The X-band EPR spectra of the complexes were recorded on a Bruker ESP 300 spectrometer at 300 K. Simulations of the spectra were performed with the simulation package employing full-matrix diagonalizations developed by Weihe.[43] Infrared and Raman (λ = 1064 nm) spectra were recorded on solid samples (KBr disks) on a Perkin-Elmer 2000 FT-IR/FT-NIR Raman spectrometer. The polarized single-crystal UV−vis spectra were recorded on a Varian Cary 5E UV−vis−NIR spectrometer.

X-ray Crystallographic Data Collection and Refinement of the Structures. Purple single crystals of **1** and yellow single crystals of **2** were mounted in sealed glass capillaries. Graphite-monochromated Mo Kα radiation (λ = 0.710 73 Å) was used throughout. Crystallographic data for the compounds are summarized in Table 8. Cell constants for **1** were obtained from a least-squares fit of the setting angles of 25 carefully centered reflections. Intensity data for this compound were collected on an Enraf-Nonius CAD4 diffractometer using the $\omega-2\theta$ scan technique. Data were corrected for Lorentz and polarization effects. Significant residual electron density up to 6.2 e Å^{-3} was located near (1 Å) the rhodium atoms. An attempt at improving this by use of absorption correction was unsuccessful, and the reported data are without absorption correction. Compound **2** was measured on a Siemens SMART CCD-detector system equipped with a cryogenic nitrogen cold stream. Cell constants were obtained from a fit of 8192 reflections. Intensity data were collected using the ω-scan technique. Corrections for Lorentz and polarization effects and a semiempirical absorption correction using the program SADABS[44] were applied. The Siemens ShelXTL[45] software package was used for solution, refinement, and artwork of the structures. All structures were solved and refined by direct methods and difference Fourier techniques performed on DEC alpha workstations. Neutral atom scattering factors were obtained from tables.[46] In **2**, disorder of one water molecule and of the anion in one site near a center of inversion was modeled with two equally populated fragments. Details are given in the Supporting Information.

Acknowledgment. This work was supported by the Fonds der Chemischen Industrie. J.B. acknowledges a traveling grant from the Ottilia and Christian Brorsons foundation. Drs. F. Galsbøl and K. P. Simonsen are thanked for donation of $[Rh(en)_3]Cl_3 \cdot 3H_2O$ and $[Rh(tn)_3]Cl_3$, respectively. R.J.D. acknowledges the support of the Engineering and Physical Sciences Research Council and the University of Warwick for the provision of computer hardware.

Supporting Information Available: Tables listing detailed crystallographic data, atomic positional parameters, and bond lengths and angles. This material is available free of charge via the Internet at http://pubs.acs.org.

IC990971J

(39) Mulliken, R. S. *J. Chem. Phys.* **1955**, *23*, 1833.
(40) Slater, J. C. *Quantum Theory of Molecules and Solids*; McGraw-Hill: New York, 1974.
(41) Ziegler, T.; Rauk, A.; Baerends, E. J. *Theor. Chim. Acta* **1977**, *43*, 261.
(42) Daul, C. *Int. J. Quantum Chem.* **1994**, *52*, 867.
(43) Weihe, H. *SIM and SIMSPEC*; University of Copenhagen: Copenhagen, 1997.
(44) Sheldrick, G. M. Universität Göttingen, 1994.
(45) *ShelXTL V. 5;* Siemens Analytical X-ray Instruments, Inc.: Madison, WI, 1994.
(46) *International Tables for X-ray Crystallography;* Kynoch Press: Birmingham, U.K., 1991.
(47) Bendix, J.; Wilson, S. R.; Prussak-Wiechowska, T. *Acta Crystallogr.* **1998**, *C53*, 923.
(48) Du Bois, J.; Hong, J.; Carreira, E. M.; Day, M. W. *J. Am. Chem. Soc.* **1996**, *118*, 915.
(49) Groves, J. T.; Takahashi, T.; Butler, W. M. *Inorg. Chem.* **1983**, *22*, 884.
(50) Buchler, J. W.; Dreher, C.; Lay, K.-L.; Lee, Y. J. A.; Scheidt, R. W. *Inorg. Chem.* **1983**, *22*, 888.